medical sciences forum

MDPI

Proceeding Paper

De Novo Drug Design of Potential Inhibitors of SARS-CoV-2 Papain-like Protease †

Edgar Clyde R. Lopez [1,2]

[1] Chemical Engineering Department, Adamson University, 900 San Marcelino St., Ermita, Manila 1000, Philippines; edgarclydelopez09@gmail.com
[2] Nanotechnology Research Laboratory, Department of Chemical Engineering, University of the Philippines Diliman, Quezon City 1101, Philippines

† Presented at the 2nd International Electronic Conference on Biomedicines, 1–31 March 2023; Available online: https://ecb2023.sciforum.net/.

Abstract: Here, potential inhibitors of the SARS-CoV-2 papain-like protease (PL^{pro}) are reported. A drug molecule (PL^{pro}-50), designed de novo using generative neural networks, interacts with PL^{pro} via hydrogen bonding, forming a salt bridge, and π–π stacking, making it a promising drug against PL^{pro}. PL^{pro}-50 has an excellent ADMET profile with good absorbability, high clearance, and low toxicity. Molecular dynamics analysis revealed the stability of the receptor–ligand complex of PL^{pro}-50 and PL^{pro}. An organic retrosynthesis study showed the feasibility of PL^{pro}-50 to be synthesized using low-cost starting materials. Further studies should be performed to determine whether the determined drug candidates are efficacious in treating COVID-19 infections.

Keywords: SARS-CoV-2; COVID-19; de novo drug design; molecular dynamics

Citation: Lopez, E.C.R. De Novo Drug Design of Potential Inhibitors of SARS-CoV-2 Papain-like Protease. *Med. Sci. Forum* **2023**, *21*, 37. https://doi.org/10.3390/ECB2023-14368

Academic Editor: Sílvia A. Sousa

Published: 23 April 2023

1. Introduction

Severe Acute Respiratory Syndrome Coronavirus 2 (SARS-CoV-2), the causative agent of the Coronavirus Disease 2019 (COVID-19) [1], caused an ongoing global pandemic that claimed over 6.9 million lives to date. Moreover, several global strategies were launched to find therapeutic agents against COVID-19 [2]. For example, known drugs could be repurposed to inhibit the progression of SARS-CoV-2 and reduce patient mortality [3,4]. Among the drugs used in the WHO solidarity trials are the antiviral drugs remdesivir, hydroxychloroquine, and a combination of lopinavir/ritonavir. However, their studies showed these drugs had little or no effect on overall mortality, ventilation initiation, and the hospital stay duration in hospitalized patients [5]. As such, there remains a need to discover possible therapeutic drugs inhibiting SARS-CoV-2.

Several strategies are available to develop drugs that target SARS-CoV-2 [6]. For example, drugs could be developed to inhibit the spike protein of SARS-CoV-2 from preventing its viral entry and halting reproduction. Hydroxychloroquine and investigational neutralizing antibodies use this principle. Another strategy is to halt the replication of SARS-CoV-2 through inhibiting the RNA polymerase, which plays a vital role in replicating and transcribing viral genomic RNA. The antiviral drugs Remdesivir and Favipinavir are promising candidates that use this strategy. A third strategy involves the inhibition of the proteases responsible for cleaving the polyproteins essential for viral replication. Such is the case for the antiviral drugs lopinavir and ritonavir [7].

Among these three key targets, the papain-like protease (PL^{pro}) of coronaviruses is among the best-characterized drug targets for drug discovery. Together with the chymotrypsin-like protease ($3CL^{pro}$), they are responsible for processing the polyproteins to generate a functional replicase complex, thus enabling viral spread. In addition, PL^{pro} can also cleave the proteinaceous post-translational modifications on host proteins, which provides an evasion mechanism against the host's antiviral immune responses. Given its

role in viral reproduction, inhibiting this enzyme would attenuate viral RNA synthesis and halt the replication of SARS-CoV-2 [8,9].

Drug discovery and development is a long and expensive process full of risks and failures. It requires a multi-disciplinary collaboration and a very high investment cost. However, rapid growth in computational drug design, high throughput screening, and combinatorial chemistry allowed us to shorten the pipeline through focusing only on promising lead candidates. Computational drug discovery is generally categorized into structure-based drug design (SBDD), ligand-based drug design (LBDD), and sequence-based approaches [10]. Structure-based drug design focuses on identifying active drug candidates (hit identification) and determining biologically active and safe candidates (lead optimization). This can be achieved through performing high-throughput virtual screening of compound libraries or designing drug molecules de novo [11–13]. On the other hand, ligand-based drug design focuses on the quantitative structure–activity relationship (QSAR), pharmacophore modeling, molecular field analysis, and 2D and/or 3D similarity assessment to rationally design molecules suitable for lead discovery and optimization [10,14,15].

Several studies have already reported candidate drug molecules based on screening several compound libraries [16,17]. Here, we report some potential SARS-CoV-2 papain-like protease inhibitors discovered using de novo drug design. These drugs may open new frontiers to possible therapies against COVID-19.

2. Computational Details

2.1. Target Preparation

The high-resolution crystal structure of PL^{pro} (PDB 6WZU) [18] was obtained from the Protein Data Bank. First, its structure was pre-processed to get its minimum-energy configuration, which was used for subsequent docking calculations. Specifically, missing hydrogens were added, correct bond orders were checked and assigned, correct protonation states were predicted, and hydrogen bonds were optimized through systematic and cluster-based approaches. In addition, restrained minimization was also applied to relax bonds, angles, and overlaps within the structure.

2.2. De Novo Drug Design

De novo drug design against the binding site of PL^{pro} was implemented using the e-LEA3D web server [19]. Lipinski's Rule of Five [20] was used as a constraint to ensure that the molecules that will be designed are drug-like [21]. A genetic algorithm was implemented with a starting population of FDA-approved drugs with a maximum population size of 40 molecules. First, the fitness of each candidate molecule is evaluated using a fitness function. Then, selection criteria are applied to choose the best candidates for breeding. Finally, breeding functions, i.e., crossover and mutation, are applied to the selected candidates to produce the next generation of solutions. These daughter solutions now become the parent solutions, and the algorithm is repeated until convergence is reached. The maximum number of generations was limited to 50 cycles to reduce computational costs [19].

De novo drug design was also implemented using the LIGANN web server to generate a library of drug-like molecules that targets PL^{pro} through generative neural networks. In particular, a generative adversarial network was used to produce complementary ligand shapes in a multimodal fashion. Then, a shape captioning network decodes the ligand shapes into SMILES strings [22]. Finally, the generated library of SMILES was converted to a structure file using Open Babel v. 3.1.1 [23]. This chemical library was then docked against the binding site of PL^{pro} using the same docking protocol described above as implemented in the LEA3D web server.

2.3. Molecular Dynamics

Ligand–protein interactional binding mode and the dynamical unbinding process through performing molecular dynamics calculations on the top-performing ligand ob-

tained from de novo drug design. The calculations were implemented using the Ligand and Receptor Molecular Dynamics (LARMD) webserver [24] for each protein–ligand complex structure. The antechamber module and the Tleap module of the AMBER16 program [25] were used to assign the bcc charges for the ligand atoms and construct the complex's coordinate and topology files. The AMBER ff14SB force field [26] and gaff force field [27,28] were used for amino acid residues and ligands. The structures are solvated using an octahedron box of TIP3P waters [29] extended at least 10 Å in each direction from the solute [30]. Na^+ and/or Cl^- ions are added to the system as counter ions. Four-step minimization of the system was achieved using the Sander module in AMBER16. Two thousand steps steepest descent method and 3000 steps conjugated gradient method were used for each minimization step. The system was then heated from 10 to 300 K in 30 ps using an NVT ensemble, followed by dynamics run at 300 K and 1 atm for 4 ns. All dynamics runs were performed using the Pmemd module of AMBER16. MD analyses were carried out using the Cpptraj module of AMBER16. MDTraj was used to calculate nonnative contact [31], and Bio3d was utilized to analyze PCA and residue cross-correlation [32] as implemented in the LARMD server.

2.4. Absorption, Distribution, Metabolism, Excretion, and Toxicity (ADMET) Study

All top-performing drug candidates were analyzed for their ADMET properties using the ADMETlab 2.0 platform. ADMETlab 2.0 is based on 53 predictive models from a comprehensively collected database of 288,867 molecules. The library of input molecules is fed into a Multi-task Graph Attention (MGA) framework to generate the ADMET profiles of each entry based on the trained regression models [33]. Only those that pass the following criteria were deemed promising lead molecules: good human intestinal absorption probability ($p > 0.7$), low blood–brain barrier probability ($p < 0.7$), low mutagenicity ($p < 0.3$), low acute toxicity ($p < 0.3$), and low carcinogenicity ($p < 0.3$).

2.5. Organic Retrosynthesis

Computer-aided organic synthesis (CAOS) of the top-performing de novo-generated inhibitors was achieved using spaya.ai—a web-based retrosynthesis tool that uses artificial intelligence to map possible reaction routes toward the desired target molecule.

3. Results and Discussion

3.1. Structure of Papain-like Protease

The minimized structure of the papain-like protease of SARS-CoV-2 is shown in Figure S1. Structurally, the papain-like protease of SARS-CoV-2 consists of 315 amino acid residues folded into four sub-domains and resembles the papain-like protease of SARS-CoV, the causative agent of a severe acute respiratory syndrome (SARS). The enzyme's active site is located at the interface between C111, H272, and D286, forming its catalytic triad. Other catalytically important residues are W93, W106, D108, and N109 [34].

3.2. De Novo Drug Design

In our attempt to discover novel drug candidates that target the papain-like protease of SARS-CoV-2, de novo drug design was performed using a genetic algorithm starting from a population of FDA-approved drugs. After fifty generations, we arrived at (2E,4E,6Z,8E)-9-[(2R,3R,4S,6R)-6-[3-(3-carboxypropyl-4-methylphenyl-3-hydroxy-2-(hydroxymethyl)oxan-4-yl]-3,7-dimethylnona-2,4,6,8-tetraenoic acid (PL^{pro}-50) as a potential inhibitor of PL^{pro}. The evolution of the solution to the genetic algorithm is shown in Figure S2a. Meanwhile, the 2D structure of PL^{pro}-50 is shown in Figure S2b. PL^{pro}-50 forms several interactions with PL^{pro}, as shown in Figure 1. Notably, its hydroxyl groups form hydrogen bonds with N109 and G27. One of its carboxylic groups forms hydrogen bonds with W106 and A288, while the other carboxylic group forms a salt bridge with K274. Moreover, its aromatic ring can interact with W106 through π–π stacking. The presence of several interactions between PL^{pro}-50 and PL^{pro} makes the complex stable, with a docking score of 95.19%.

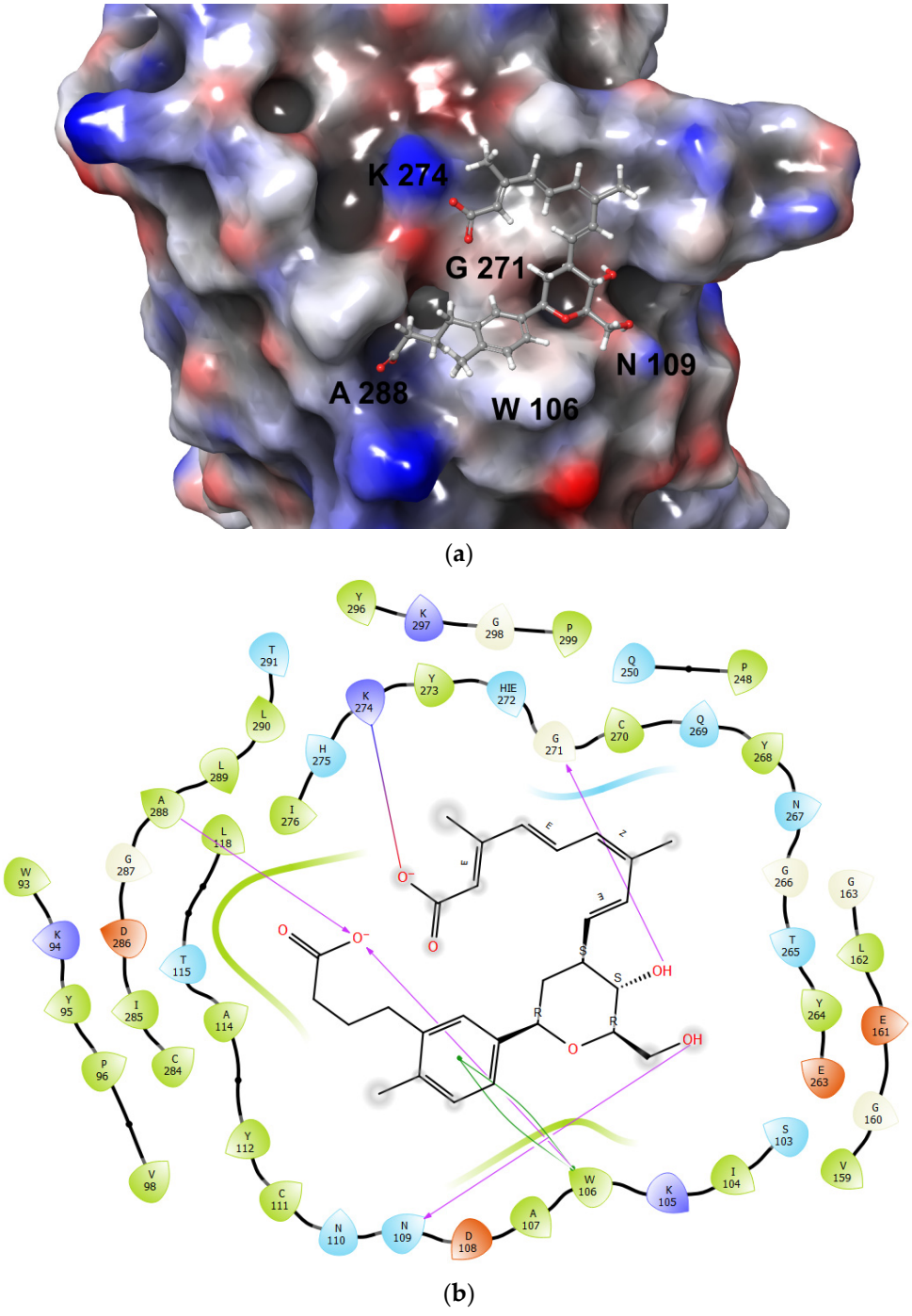

Figure 1. Interaction of PL^{pro} with PL^{pro}−50: (**a**) structure of the PL^{pro}−PL^{pro}−-50 complex; (**b**) ligand interaction diagram.

In another method, 722 drug-like molecules were generated using generative neural networks. This is more robust than using a genetic algorithm with a starting population of FDA-approved drugs since the former can capture a wider area within the chemical space. Figure S1 shows the top-performing molecules after docking the generated chemical library against the binding site of PL^{pro}. Among them, only 6WZU-1 and 6WZU-11 have ideal ADMET profiles. Hence, we further focused on investigating the inhibitory properties of these two lead molecules.

6WZU-1, whose IUPAC name is (2-phenylethyl)[2-(pyridin-2-yl)ethyl]{[(3R)-1-{[(3S)-1,2,3,4-tetrahydro-1,5-naphthyridin-3-yl]methyl}piperidin-3-yl]methyl}amine, forms a hy-

drogen bond with D286. Meanwhile, 6WZU-11 or [(2R)-6-aminohexan-2-yl][(1R)-1-[5-(1-benzylpiperidin-4-yl)-1,3-thiazol-2-yl]ethyl]amine forms hydrogen bonds with D108 and N109. Its five-membered ring also interacts with W106 via π–π stacking. The corresponding docked structures of these two molecules are shown in Figures 2 and 3, respectively. Due to these ligand–residue interactions, we see that 6WZU-1 and 6WZU-11 have the potential to inhibit PL^{pro}-50.

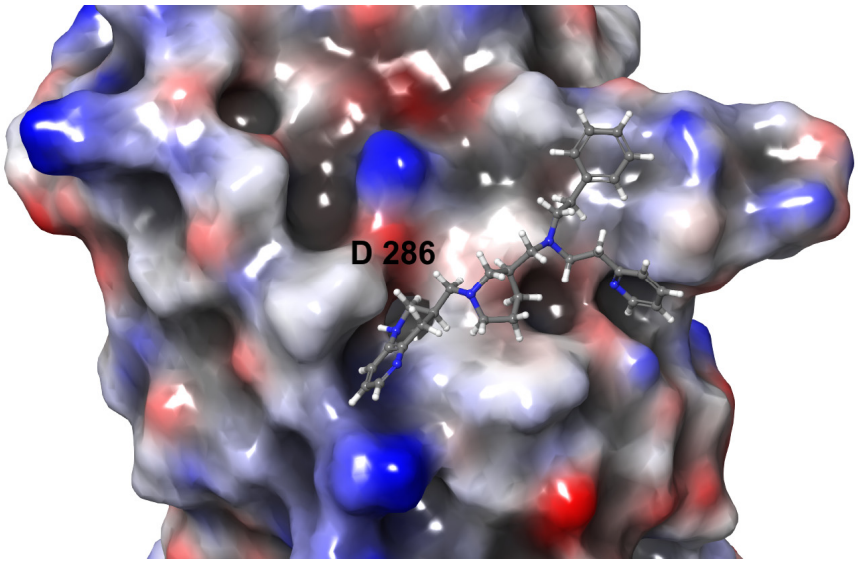

(**a**)

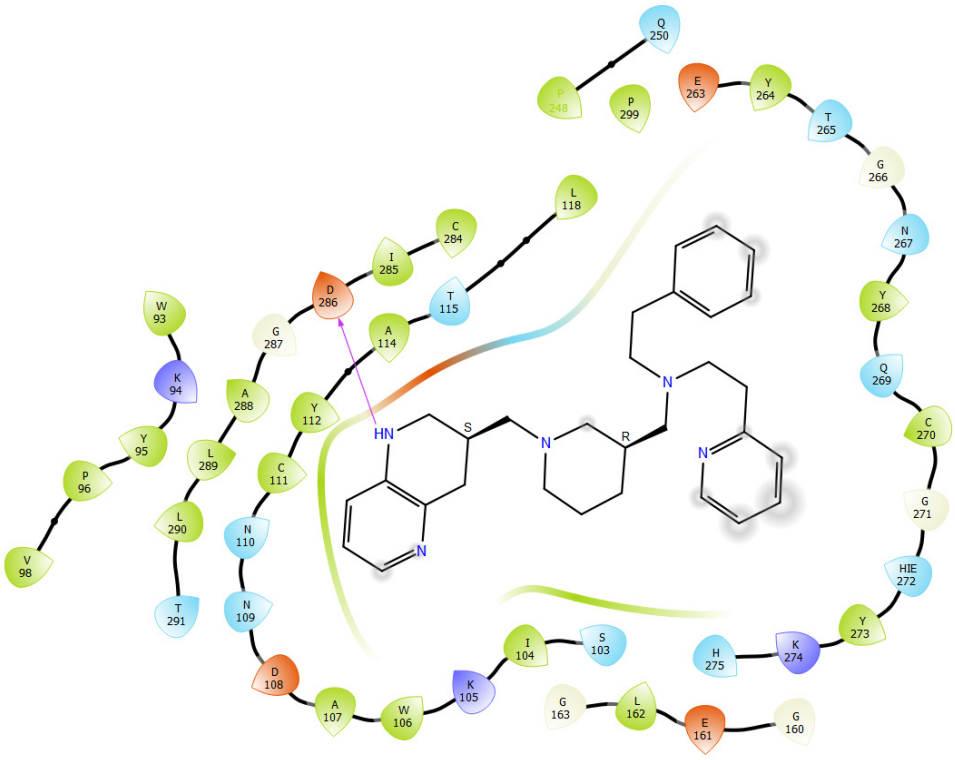

(**b**)

Figure 2. Interaction of PL^{pro} with 6WZU-1: (**a**) structure of the PL^{pro}-6WZU-1 complex; (**b**) ligand interaction diagram.

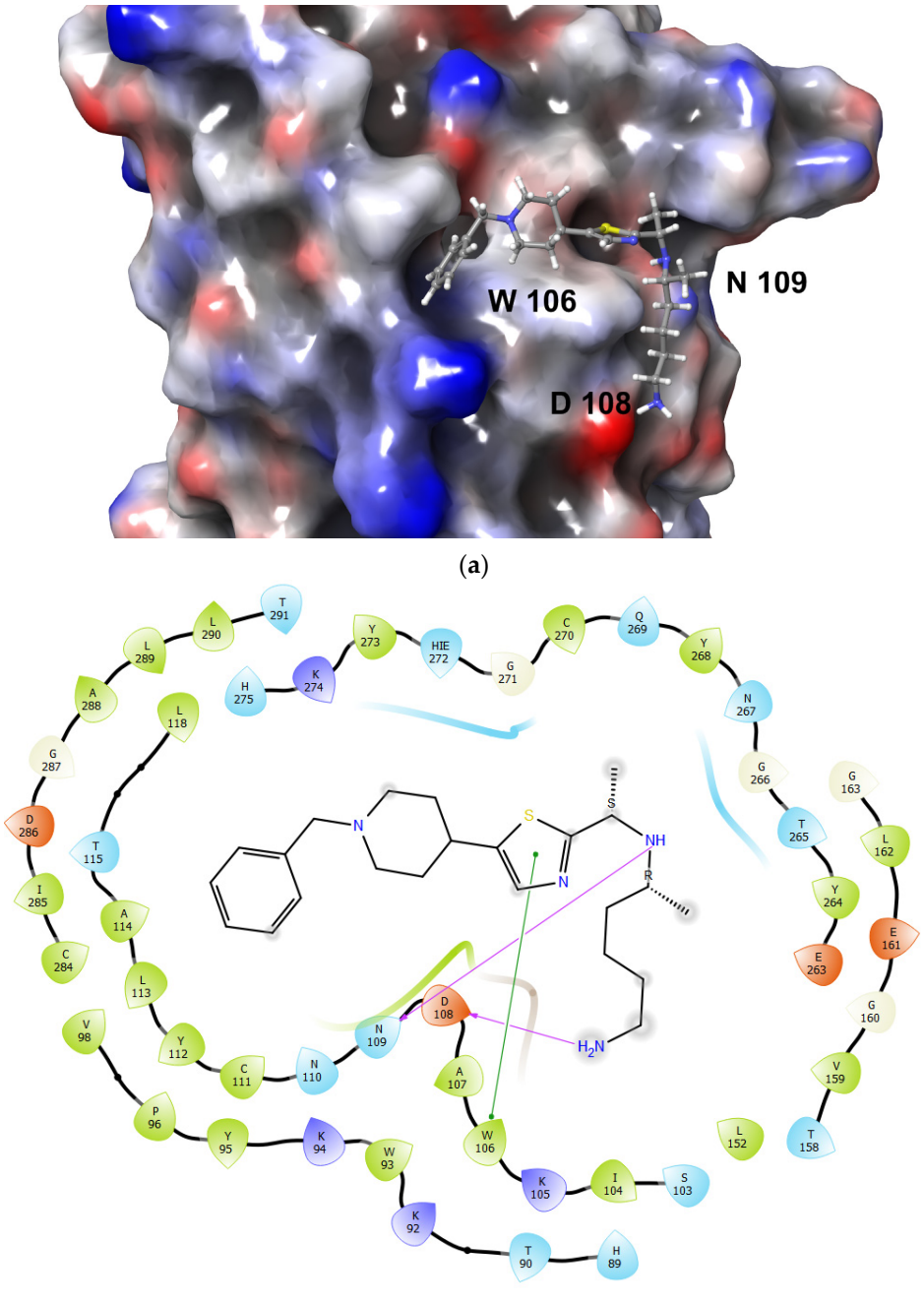

Figure 3. Interaction of PL^{pro} with 6WZU-11: (**a**) structure of the PL^{pro}-6WZU-11 complex; (**b**) ligand interaction diagram.

3.3. Molecular Dynamics Analysis

To further understand the inhibitory effect of PL_{pro}-50, we performed a molecular dynamics simulation on the docked protein–ligand structure. Shown in Figure S4 are the RMSD profile and histograms of the docked structure over time. Our data revealed that the docked structure equilibrated well after 3 ns of MD simulation with a receptor average RMSD of 1.2379 ± 0.2578 Å and a ligand average RMSD of 2.8021 ± 0.7697 Å. The RMSD values of the receptor and the ligand are normally distributed. The hydrogen bonds between PL^{pro}-50 and the protease residues W106 and A288 comprise most of the population of hydrogen bonds formed and are well-maintained throughout the dynamics run, indicating the docked stability structure. A strong binding energy (ΔG_{PB} = −7.63 kcal mol^{-1} and ΔG_{GB} = −7.57 kcal mol^{-1})

was calculated for the docked PL^{pro}-50 complex, indicating the good inhibitory property of PL^{pro}-50.

Principal component analysis of PL^{pro}-50 binding (Figure S5) and unbinding (Figure S6) and their corresponding dynamic cross-correlation analysis (Figure S7) were determined based on their corresponding MD trajectories. Only the top three principal components are presented in the figure because these are generally sufficient to capture approximately 50% of the total variance in a given family of structures [29]. Our results show no significant difference between the conformations of PL^{pro}-50 during the ligand-protein interactional binding and the dynamical unbinding process, indicating the stability of the resulting ligand-protein structure. This further reinforces our hypothesis that PL^{pro}-50 could inhibit SARS-CoV-2's papain-like protease.

3.4. Organic Retrosynthesis

The main issue with the de novo design of ligands for inhibiting a particular protein is whether they can be synthesized in the real world. Therefore, we calculated the synthetic accessibility scores (SAscore) of all the compounds in this study to ascertain their synthetic feasibility. SAscore is a scoring function based on a combination of fragment contributions and a complexity penalty [35]. Our results showed that all of our top-performing ligands have excellent synthetic accessibility scores (SAscore < 6), indicating that it is possible to synthesize these molecules.

To demonstrate that our top de novo-generated drug-like molecules can be synthesized in the laboratory, we employed artificial intelligence to map out possible reaction routes to synthesize the said molecules using commercially available starting materials. For example, PL^{pro}-50 may be synthesized using ten major reactions involving 3-methyl but-2-enal, 3-methyl but-2-enoic acid, 4-butyrolactone, 3,4-dihydro-2H-pyran-4-one, and toluene as starting materials, as outlined in Scheme S1. Meanwhile, 6WZU-1 may be synthesized using 2-(3-nitropyridin-2-yl)acetic acid, acetophenone, 1-(piperidin-3-yl)methanamine, and 2-hydroxypyridine as starting materials involving 11 major chemical steps as shown in Scheme S2. Moreover, 6WZU-11 may be synthesized using acetyl chloride, hexane-1,5-diamine, methoxy(methyl)amine, benzyl alcohol, 4-hydroxy-piperidine, and 1,3-thiazole as starting materials. The entire pathway comprises eight major reactions, as shown in Scheme S3. To further assist the synthesis of our de novo-designed drug-like molecules, we also included their corresponding predicted ^{1}H NMR and ^{13}C NMR in Figures S14 and S15, respectively. NMR predictions were made using ChemAxon's Marvin Sketch 21.4.0.

4. Conclusions

Potential inhibitors of the SARS-CoV-2 papain-like protease (PL^{pro}) were discovered using de novo drug design. We report a drug molecule (PL^{pro}-50) designed de novo through performing a genetic algorithm search using an initial population of FDA-approved drugs. After fifty generations, PL^{pro}-50 emerged as a strong candidate and demonstrated to be a potentially better inhibitor against PL^{pro} than the top-performing FDA-approved drugs. We also designed a chemical library of potential inhibitors of PL^{pro}, of which 6WZU-1 and 6WZU-11 emerged superior over the other drug-like molecules. These drug molecules merit further studies to demonstrate whether their in silico performance translates to clinical efficacy and safety.

Supplementary Materials: The following supporting information can be downloaded at: https://www.mdpi.com/article/10.3390/ECB2023-14368/s1, Figure S1. Structure of the main protease (PL^{pro}) showing its (a) secondary structure and (b) catalytic triad (binding pocket).; Figure S2. (a) Evolution of docking score during the de novo design of PL^{pro} inhibitors using genetic algorithm; (b) chemical structure of PL^{pro}-50 drawn using ChemAxon Marvin Suite.; Figure S3. Top-performing drug-like molecules to inhibit PL^{pro}.; Figure S4. (a) RMSD profile of the docked PL^{pro}-50 ligand in PL^{pro}, (b) RMSD histogram of the receptor, and (c) RMSD histogram of the ligand.; Figure S5. (a) Principal Component Analysis (PCA) for the MD trajectory of PL^{pro}-50 binding into PL^{pro}. (b) Simple clustering in PC subspace.; Figure S6. (a) Principal Component Analysis (PCA) for the MD trajectory

of the unbinding process between PL^{pro}-50 and PL^{pro}.; Figure S7. Dynamical residue cross-correlation map for the MD trajectory of the (a) binding process and (b) unbinding process of the receptor-ligand complex involving PL^{pro}-50 docked in PL^{pro}.; Figure S8. Residue-wise loading for (a) PC1, (b) PC2, and (c) PC3 of the binding process of the receptor-ligand complex involving PL^{pro}-50 docked in PL^{pro}. Residue-wise loading for (d) PC1, (e) PC2, (f) PC3 of the unbinding process of the receptor-ligand complex involving PL^{pro}-50 docked in PL^{pro}.; Table S1. ADMET profiles of top-performing FDA-approved drugs as PL^{pro} inhibitors.; Table S2. Interacting residues of PL^{pro} with its potential inhibitors.; Figure S9. (a) RMSD profile of the docked 6WZU-11 in PL^{pro}. and (c) RMSD histogram of the ligand (mean RMSD = 2.0645 $\pm$ 0.0057 Å).; Figure S10. (a) Principal Component Analysis (PCA) for the MD trajectory of 6WZU-11 binding into PL^{pro}. (b) Simple clustering in PC subspace.; Figure S11. (a) Principal Component Analysis (PCA) for the MD trajectory of the unbinding process between 6WZU-11 and PL^{pro}. (b) Simple clustering in PC subspace.; Figure S12. Dynamical residue cross-correlation map for the MD trajectory of the (a) binding process and (b) unbinding process of the receptor-ligand complex involving 6WZU-11 docked in PL^{pro}.; Figure S13. Residue-wise loading for (a) PC1, (b) PC2, (c) PC3 of the binding process of the receptor-ligand complex involving 6WZU-11 docked in PL^{pro}. Residue-wise loading for (d) PC1, (e) PC2, (f) PC3 of the unbinding process of the receptor-ligand complex involving PL^{pro}-50 docked in PL^{pro}.; Figure S14. Predicted ^{1}H NMR of (a) PL^{pro}-50, (b) 6WZU-1, and (c) 6WZU-11.; Figure S15. Predicted ^{13}C NMR at 500.0 MHz of (a) PL^{pro}-50, (b) 6WZU-1, and (c) 6WZU-11.; Scheme S1. Proposed synthesis route for PL^{pro}-50.; Scheme S2. Proposed synthesis route for 6WZU-1.; Scheme S3. Proposed synthesis route for 6WZU-11.

Funding: This research received no external funding.

Institutional Review Board Statement: Not applicable.

Informed Consent Statement: Not applicable.

Data Availability Statement: The data presented in this study are available in the Supplementary Material.

Conflicts of Interest: The authors declare no conflict of interest.

References

1. Gorbalenya, A.E.; Baker, S.C.; Baric, R.S.; de Groot, R.J.; Drosten, C.; Gulyaeva, A.A.; Haagmans, B.L.; Lauber, C.; Leontovich, A.M.; Neuman, B.W.; et al. The species Severe acute respiratory syndrome-related coronavirus: Classifying 2019-nCoV and naming it SARS-CoV-2. *Nat. Microbiol.* **2020**, *5*, 536–544. [CrossRef]
2. Bouyahya, A.; El Omari, N.; Elmenyiy, N.; Hakkour, M.; Balahbib, A.; Guaouguaou, F.E.; Benali, T.; El Baaboua, A.; Belmehdi, O. Therapeutic strategies of COVID-19: From natural compounds to vaccine trials. *Biointerface Res. Appl. Chem.* **2021**, *11*, 8318–8373. [CrossRef]
3. Hazafa, A.; Ur-Rahman, K.; Haq, I.-U.; Jahan, N.; Mumtaz, M.; Farman, M.; Naeem, H.; Abbas, F.; Naeem, M.; Sadiqa, S.; et al. The broad-spectrum antiviral recommendations for drug discovery against COVID-19. *Drug Metab. Rev.* **2020**, *52*, 408–424. [CrossRef] [PubMed]
4. Yousefi, H.; Mashouri, L.; Okpechi, S.C.; Alahari, N.; Alahari, S.K. Repurposing existing drugs for the treatment of COVID-19/SARS-CoV-2 infection: A review describing drug mechanisms of action. *Biochem. Pharmacol.* **2021**, *183*, 114296. [CrossRef] [PubMed]
5. WHO Solidarity Trial Consortium. Repurposed Antiviral Drugs for COVID-19—Interim WHO Solidarity Trial Results. *N. Engl. J. Med.* **2021**, *384*, 497–511. [CrossRef] [PubMed]
6. Chellapandi, P.; Saranya, S. Genomics insights of SARS-CoV-2 (COVID-19) into target-based drug discovery. *Med. Chem. Res.* **2020**, *29*, 1777–1791. [CrossRef]
7. Jeong, G.U.; Song, H.; Yoon, G.Y.; Kim, D.; Kwon, Y.-C. Therapeutic Strategies Against COVID-19 and Structural Characterization of SARS-CoV-2: A Review. *Front. Microbiol.* **2020**, *11*, 1723. [CrossRef]
8. Shin, D.; Mukherjee, R.; Grewe, D.; Bojkova, D.; Baek, K.; Bhattacharya, A.; Schulz, L.; Widera, M.; Mehdipour, A.R.; Tascher, G.; et al. Papain-like protease regulates SARS-CoV-2 viral spread and innate immunity. *Nature* **2020**, *587*, 657–662. [CrossRef]
9. Maiti, B.K. Can Papain-like Protease Inhibitors Halt SARS-CoV-2 Replication? *ACS Pharmacol. Transl. Sci.* **2020**, *3*, 1017–1019. [CrossRef]
10. Ou-Yang, S.; Lu, J.; Kong, X.; Liang, Z.; Luo, C.; Jiang, H. Computational drug discovery. *Acta Pharmacol. Sin.* **2012**, *33*, 1131–1140. [CrossRef]
11. Bechelane-Maia, E.H.; Assis, L.C.; Alves de Oliveira, T.; Marques da Silva, A.; Gutterres Taranto, A. Structure-based virtual screening: From classical to artificial intelligence. *Front. Chem.* **2020**, *8*, 343. [CrossRef]

12. Lionta, E.; Spyrou, G.; Vassilatis, D.K.; Cournia, Z. Structure-Based Virtual Screening for Drug Discovery: Principles, Applications and Recent Advances. *Curr. Top. Med. Chem.* **2014**, *14*, 1923–1938. [CrossRef]
13. Danishuddin, M.; Khan, A.U. Structure based virtual screening to discover putative drug candidates: Necessary considerations and successful case studies. *Methods* **2015**, *71*, 135–145. [CrossRef]
14. Tresadern, G.; Bemporad, D. Modeling approaches for ligand-based 3D similarity. *Futur. Med. Chem.* **2010**, *2*, 1547–1561. [CrossRef]
15. Acharya, C.; Coop, A.; Polli, J.E.; MacKerell, A.D. Recent advances in ligand-based drug design: Relevance and utility of the conformationally sampled pharmacophore approach. *Curr. Comput. Aided-Drug Des.* **2010**, *7*, 10–22. [CrossRef]
16. Gupta, A.; Rani, C.; Pant, P.; Vijayan, V.; Vikram, N.; Kaur, P.; Singh, T.P.; Sharma, S.; Sharma, P. Structure-Based Virtual Screening and Biochemical Validation to Discover a Potential Inhibitor of the SARS-CoV-2 Main Protease. *ACS Omega* **2020**, *5*, 33151–33161. [CrossRef]
17. Carli, M.; Sormani, G.; Rodriguez, A.; Laio, A. Candidate Binding Sites for Allosteric Inhibition of the SARS-CoV-2 Main Protease from the Analysis of Large-Scale Molecular Dynamics Simulations. *J. Phys. Chem. Lett.* **2020**, *12*, 65–72. [CrossRef] [PubMed]
18. Osipiuk, J.; Azizi, S.-A.; Dvorkin, S.; Endres, M.; Jedrzejczak, R.; Jones, K.A.; Kang, S.; Kathayat, R.S.; Kim, Y.; Lisnyak, V.G.; et al. Structure of papain-like protease from SARS-CoV-2 and its complexes with non-covalent inhibitors. *Nat. Commun.* **2021**, *12*, 1–9. [CrossRef] [PubMed]
19. Douguet, D. e-LEA3D: A computational-aided drug design web server. *Nucleic Acids Res.* **2010**, *38*, 615–621. [CrossRef]
20. Lipinski, C.A. Drug-like properties and the causes of poor solubility and poor permeability. *J. Pharmacol. Toxicol. Methods* **2000**, *44*, 235–249. [CrossRef] [PubMed]
21. Benet, L.Z.; Hosey, C.M.; Ursu, O.; Oprea, T.I. BDDCS, the Rule of 5 and drugability. *Adv. Drug Deliv. Rev.* **2016**, *101*, 89–98. [CrossRef] [PubMed]
22. Skalic, M.; Jiménez, J.; Sabbadin, D.; De Fabritiis, G. Shape-Based Generative Modeling for de Novo Drug Design. *J. Chem. Inf. Model.* **2019**, *59*, 1205–1214. [CrossRef]
23. O'Boyle, N.M.; Banck, M.; James, C.A.; Morley, C.; Vandermeersch, T.; Hutchison, G.R. Open babel: An open chemical toolbox. *J. Cheminform.* **2011**, *3*, 33. [CrossRef] [PubMed]
24. Yang, J.-F.; Wang, F.; Chen, Y.-Z.; Hao, G.-F.; Yang, G.-F. LARMD: Integration of bioinformatic resources to profile ligand-driven protein dynamics with a case on the activation of estrogen receptor. *Briefings Bioinform.* **2019**, *21*, 2206–2218. [CrossRef] [PubMed]
25. Case, D.A.; Cheatham, T.E., III; Darden, T.; Gohlke, H.; Luo, R.; Merz, K.M., Jr.; Onufriev, A.; Simmerling, C.; Wang, B.; Woods, R.J. The Amber biomolecular simulation programs. *J. Comput. Chem.* **2005**, *26*, 1668–1688. [CrossRef]
26. Maier, J.A.; Martinez, C.; Kasavajhala, K.; Wickstrom, L.; Hauser, K.E.; Simmerling, C. ff14SB: Improving the accuracy of protein side chain and backbone parameters from ff99SB. *J. Chem. Theory Comput.* **2015**, *11*, 3696–3713. [CrossRef]
27. Wang, J.; Wolf, R.M.; Caldwell, J.W.; Kollman, P.A.; Case, D.A. Development and testing of a general amber force field. *J. Comput. Chem.* **2004**, *25*, 1157–1174. [CrossRef]
28. Wang, B.; Merz, K.M. A Fast QM/MM (Quantum Mechanical/Molecular Mechanical) Approach to Calculate Nuclear Magnetic Resonance Chemical Shifts for Macromolecules. *J. Chem. Theory Comput.* **2006**, *2*, 209–215. [CrossRef] [PubMed]
29. Price, D.J.; Brooks, C.L. A modified TIP3P water potential for simulation with Ewald summation. *J. Chem. Phys.* **2004**, *121*, 10096–10103. [CrossRef]
30. Jorgensen, W.L.; Chandrasekhar, J.; Madura, J.D.; Impey, R.W.; Klein, M.L. Comparison of simple potential functions for simulating liquid water. *J. Chem. Phys.* **1983**, *79*, 926–935. [CrossRef]
31. McGibbon, R.T.; Beauchamp, K.A.; Harrigan, M.P.; Klein, C.; Swails, J.M.; Hernández, C.X.; Schwantes, C.R.; Wang, L.-P.; Lane, T.J.; Pande, V.S. MDTraj: A Modern Open Library for the Analysis of Molecular Dynamics Trajectories. *Biophys. J.* **2015**, *109*, 1528–1532. [CrossRef] [PubMed]
32. Grant, B.J.; Rodrigues, A.P.; ElSawy, K.M.; McCammon, J.A.; Caves, L.S. Bio3d: An R package for the comparative analysis of protein structures. *Bioinformatics* **2006**, *22*, 2695–2696. [CrossRef] [PubMed]
33. Dong, J.; Wang, N.-N.; Yao, Z.-J.; Zhang, L.; Cheng, Y.; Ouyang, D.; Lu, A.-P.; Cao, D.-S. ADMETlab: A platform for systematic ADMET evaluation based on a comprehensively collected ADMET database. *J. Cheminform.* **2018**, *10*, 29. [CrossRef]
34. Gao, X.; Qin, B.; Chen, P.; Zhu, K.; Hou, P.; Wojdyla, J.A.; Wang, M.; Cui, S. Crystal structure of SARS-CoV-2 papain-like protease. *Acta Pharm. Sin. B* **2020**, *11*, 237–245. [CrossRef]
35. Ertl, P.; Schuffenhauer, A. Estimation of synthetic accessibility score of drug-like molecules based on molecular complexity and fragment contributions. *J. Cheminform.* **2009**, *1*, 1–11. [CrossRef] [PubMed]